J. Phys. D: Appl. Phys. **33** (2000) 1323–1331. Printed in the UK PII: S0022-3727(00)10770-3

On the plasma parameters of a planar inductive oxygen discharge

J T Gudmundsson†, A M Marakhtanov‡, K K Patel‡§, V P Gopinath‡‖ and M A Lieberman‡

† Science Institute, University of Iceland, Dunhaga 3, IS-107 Reykjavík, Iceland
‡ Department of Electrical Engineering and Computer Sciences, University of California, Berkeley, CA 94720, USA

Received 7 January 2000, in final form 21 February 2000

Abstract. Langmuir probes and a quadrupole mass spectrometer were used to determine the plasma parameters of an oxygen plasma in a planar inductive discharge. The electron density, effective electron temperature, the dc plasma potential and the electron energy probability function (EEPF) in the discharge centre plane were investigated as functions of power, gas pressure and radial position. The ion energy distribution and relative density of positive ions at the radial sheath edge were investigated as functions of power and pressure. A volume-averaged global model of the electronegative oxygen discharge is developed. The model uses a power balance equation to account for energy deposited into the plasma and lost via collisions and particle flux. The particle densities are modelled via rate equations estimated from collision cross sections assuming Maxwellian electron energy distribution functions. The volume-averaged model is shown to predict the experimental trends over a range of process conditions.

1. Introduction

Oxygen discharges have been applied in plasma processing since the early days, with applications such as ashing of photoresists [1], removing polymer films and oxidation or deposition of thin-film oxides [2, 3]. Larger wafer sizes and smaller electronic devices have led to the development of high-density plasma reactors such as inductively coupled discharges which can provide high-density plasma of good uniformity with low and controllable ion bombarding energy. In an inductive source the plasma is created by applying rf voltage to a non-resonant inductive coil, resulting in the capacitive breakdown of the process gas within or near the coil. With an increase in power the plasma is maintained inductively by the induced electric field. Typically these inductive discharges are operated at pressures between 1 and 50 mTorr and applied power between 200 and 1000 W with typical electron densities in the range of 10^{16}–10^{18} m^{-3}.

Oxygen is a simple diatomic gas, however, in an oxygen discharge a number of species are formed. The relative simplicity of oxygen in comparison with other electronegative processing gases and the presence of databases of reaction rate constants [4, 5] make oxygen discharges a good subject for modelling and experimental investigation. Oxygen plasmas in inductive discharges have been experimentally characterized by several groups. Barnes *et al* [6], Keller *et al* [7] and Schwabedissen *et al* [8] measured the electron density and the electron energy distribution function using a Langmuir probe. Tuszewski *et al* investigated the ionic composition, plasma parameters [9] and instabilities [10] of oxygen plasmas in inductive discharges. Furthermore, the ion energetics of planar inductive oxygen discharge have been investigated [11]. The volume-averaged global model for high-density discharges was developed by Lieberman and Gottscho [12] for noble gases and extended to molecular gases by Lee *et al* [13] and Lee and Lieberman [14]. The simple noble gas model was compared to Langmuir probe measurements performed on a cylindrical argon discharge with variable aspect (length/diameter) ratios [15]. A more elaborate volume-averaged global model of Ar/O_2 mixture has been developed and compared to Langmuir probe and mass spectrometer measurements [16]. The main idea of a global model is to neglect the complexity that arises when spatial variations are considered and to generate a model that encompasses large number of reactions in order to model a processing plasma with a limited computing power. We will describe measurements of plasma parameters by a Langmuir probe and ionic composition by a mass spectrometer and compare the measured values to calculated plasma parameters using a global (volume-averaged model) of oxygen discharges.

2. Experimental apparatus

The set-up of the experiment includes a planar inductively coupled plasma source, a quadrupole mass spectrometer (QMS) and a Langmuir probe measurement system. The plasma chamber consists of an anodized aluminium cylinder

§ Present address: Cypress Semiconductor, 2401 E. 86th Street, Bloomington, MN 55425, USA.
‖ Present address: LSI Logic, Process Technology Development, 3115 Alfred Street, Santa Clara, CA 95123, USA.

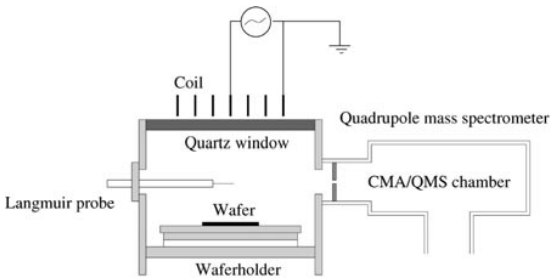

Figure 1. Schematic diagram of the planar inductive discharge and the mass spectrometer.

with inner diameter 30.48 cm and length of 1 m. Moveable aluminium pistons are at both ends. An aluminium electrode, 27 cm in diameter is mounted on one of these pistons. The electrode serves as a wafer holder and can be water cooled. A 2.5 cm thick by 25 cm diameter quartz plate mounted on the other piston separates the planar spiral induction coil from the plasma. Figure 1 shows a schematic diagram of the planar inductive plasma source and the QMS.

In all the experiments described the plasma is created inside a cylindrical vacuum chamber of radius $R = 15.24$ cm and length $L = 7.62$ cm and the diagnostic ports are in the midplane of the chamber. The plasma chamber is evacuated by a Leybold Turbovac 361C turbomolecular pump which has a pumping speed 340–400 l s^{-1} backed by a W M Welch rotary pump giving a base pressure of about 3–9 $\times$ 10^{-6} Torr. The flow rate is controlled via a Tylan PC-2900V flow controller. The flow rates were varied in the range 10–85 sccm (sccm denotes cubic centimetres per minute at standard temperature and pressure) to give pressure in the range of 3–45 mTorr. The equilibrium gas pressure in the chamber is monitored with an MKS Baratron capacitance manometer model 127 connected to a MKS Type PDR-C-2C power supply digital readout. To further control the chamber pressure the gate valve was manually adjusted to vary the pumping speed.

The source is powered at 13.56 MHz using a 1 kW Henry 1000D rf power generator connected to an L-type capacitive matching network. The power supply operates in the range 0–1000 W. The power absorbed by the plasma was determined by first measuring the transmitted power without plasma and then subtracting that power from the power transmitted with plasma present at the same current. For all measurements the aluminium plasma chamber, electrodes and pistons are grounded.

A cylindrical Langmuir probe with a separate reference electrode is used in the experiment [17]. The measurement probe is a cylindrical tungsten rod and the probe tip length 4 mm and its radius 63.5 μm. The probe holder is an alumina tube 0.5 mm in outer radius. The reference probe is a wire loop 2 cm in radius made of 0.5 mm diameter tungsten wire. The reference loop is not closed and its structure is kept by an insulating holder. A sawtooth voltage with a sweeping time of 5 ms is applied over a 50 V range to measure the probe characteristics. The measured I–V curve was smoothed by convoluting a Blackman window to the measured data [18]. The second derivative of the I–V curve is calculated and the electron energy distribution function $g_e(\mathcal{E})$ is found. The electron energy distribution function is given by the Druyvesteyn formula as [19, 20]

$$g_e(V) = \frac{2m}{e^2 A_{pr}} \left(\frac{2eV}{m}\right)^{1/2} \frac{d^2 I_e}{dV^2} \tag{1}$$

and the electron energy probability function is

$$g_p(\mathcal{E}) = \mathcal{E}^{-1/2} g_e(\mathcal{E}) \tag{2}$$

where $\mathcal{E}$ is the electron energy in equivalent voltage units. The plasma potential V_{pl} is the voltage where the second derivative of the electron current I_e is zero. The electron density n_e is determined as

$$n_e = \int_0^\infty g_e(\mathcal{E})\, d\mathcal{E} \tag{3}$$

and the effective electron temperature T_{eff} is determined as

$$T_{eff} = \frac{1}{n_e}\frac{2}{3}\int_0^\infty \mathcal{E} g_e(\mathcal{E})\, d\mathcal{E}. \tag{4}$$

We find that the smoothing method introduces distortion to the electron energy distribution function. To minimize the effect of this distortion on the electron density and effective electron temperature, the measured electron energy distribution functions are fitted to the function $g_R(\mathcal{E}) = a\sqrt{\mathcal{E}}\exp(-b\mathcal{E}^x)$ where a, b and x are constants. The Maxwellian electron energy distribution is a special case with $x = 1$ and the Druyvesteyn distribution is a special case with $x = 2$. The value of x was determined by performing a least-squares analysis of $\ln(g_R(\mathcal{E})/\sqrt{\mathcal{E}})$ against $\mathcal{E}^x$ for various x to find the best fit. The maximum of the electron energy distribution function is found and the corresponding electron energy. The equation is fitted to the measured electron energy distribution function from the electron energy where the electron energy distribution function has maximum value until it has fallen two orders of magnitude. The best fit to the equation is then interpolated to zero electron energy, and the electron density and effective electron temperature are calculated.

Mass spectrometers are useful tools in the chemical analysis of process plasmas. The mass spectrometer is connected to a diagnostic port on the circumference in the midplane of the chamber (see figure 1). Particle flux analysis is performed by extracting a particle stream (positive ions) through a 50 μm diameter sampling aperture. After extraction from the plasma the particle flux is energy analysed. The energy spectrum of each ion is then integrated to find relative ion intensity. The analysis of the ions in the plasma was performed with a SXP 300 VG QMS with a CMX 500 cylindrical mirror energy analyser [21].

3. Experimental results

A Langmuir probe was applied to measure the electron energy distribution function of the oxygen plasma. The electron energy probability function at the centre of the discharge is shown in figure 2 for an oxygen discharge at 720 W and 2.5, 10, 20 and 35 mTorr. The electron energy distribution function is close to Maxwellian over the pressure range

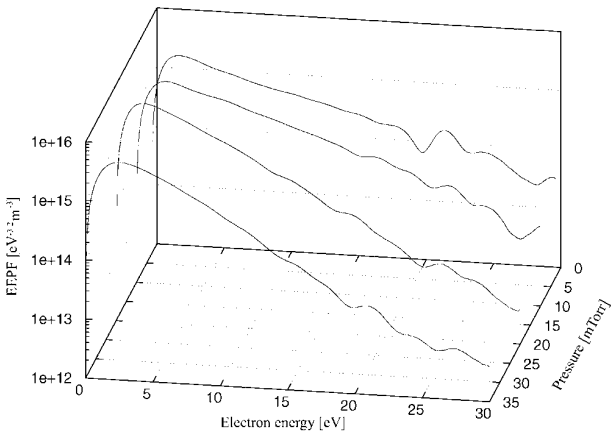

Figure 2. The electron energy probability function in the centre of an oxygen discharge at 720 W measured by a Langmuir probe at 2.5, 10, 20 and 35 mTorr pressure.

investigated. The parameter x is 1.06 at 2.5 mTorr and increases with increased pressure to about 1.25 at 35 mTorr. Thus the plasma is Maxwellian at low pressure, but becomes more Druyvesteyn as the pressure is increased. The plasma parameters electron density, effective electron temperature and the dc plasma potential in the discharge centre were calculated from the Langmuir probe I–V characteristic and are shown in figure 3. The electron density n_e and the effective electron temperature T_{eff} are calculated as integrals over the electron energy distribution function using equations (3) and (4), respectively. Experiments were conducted at several flow rates and pressures over the power range 0–800 W. The electron density n_e is shown against power in figure 3(a). The electron density increases linearly with increasing power which is consistent with what is commonly observed in inductive discharges [7]. The effective electron temperature in figure 3(b) and the dc plasma potential in figure 3(c) are nearly independent of the power but increase with decreasing pressure. There was no sign of negative ions in the measured Langmuir probe I–V curve. Radial measurements of the electron energy probability function and the plasma parameters are shown in figures 4 and 5 respectively. The measurements are all performed in the midplane of the chamber. The radial dependence of the electron energy probability function at 720 W and 5 mTorr ($q = 25$ sccm) is shown in figure 4. The electron energy distribution is close to Maxwellian over the radius of the chamber. The parameter x is 1.2 at the centre of the discharge and 1.1 at $r/R = 0.85$. The radial dependence of the plasma parameters is shown in figure 5. We observe an off-axis electron density peak over the pressure range of interest. The electron density shown in figure 5(a) increases from the centre plane of the discharge and peaks at roughly $r/R = 0.5$. As discussed by Hopwood *et al* [22], Meyer and Wendt [23] and Meyer *et al* [24] the inductive electric field and thus the absorbed power peak at approximately one-half the radius of the coil and go to zero in the centre of the discharge. The effective electron temperature, shown in figure 5(b), increases slightly towards the chamber wall.

The ion energy distributions of positive ions bombarding the walls were recorded for various pressure and power

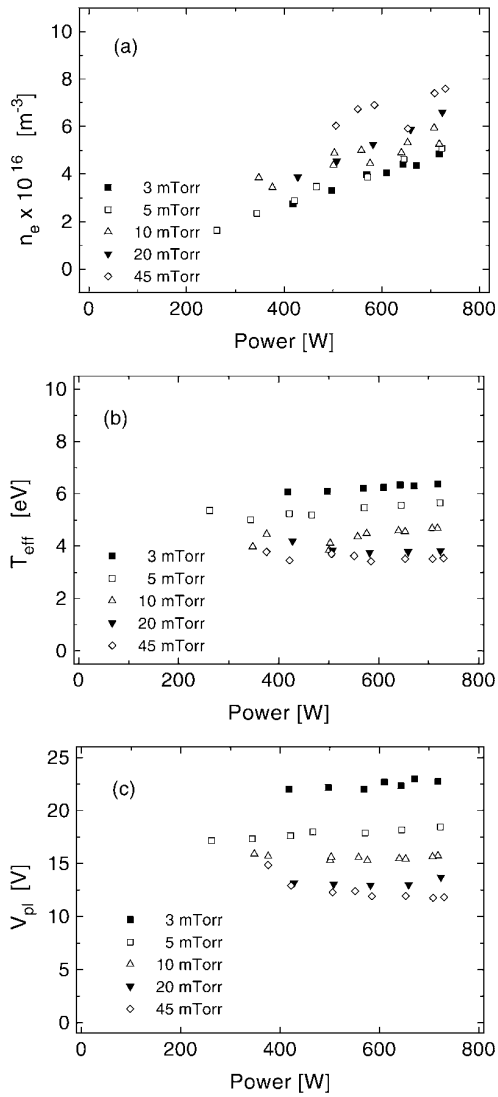

Figure 3. Plasma parameters in the centre of an oxygen discharge at 720 W measured by a Langmuir probe, (a) electron density n_e, (b) effective electron temperature T_{eff} and (c) dc plasma potential V_{pl}.

values. A detailed discussion of the ion energy distribution in oxygen discharges is given elsewhere [11]. The normalized ion energy distribution for O^+ and O_2^+ ions in oxygen plasma at 675 W is shown in figure 6 for pressures 3, 7 and 20 mTorr. The ion energy distribution is normalized such that the area under the distribution is one. As the pressure is increased the mean ion energy decreases and the width of the ion energy distribution decreases. At low pressure (3 mTorr), the high-energy peak dominates. With increasing pressure the high-energy peak decreases and moves to lower energies and finally disappears, resulting in only one peak with mean ion energy of roughly 10 eV for O^+ ions and 12 eV for O_2^+ ions at 20 mTorr. As the pressure is increased the ion–neutral mean free path decreases and becomes of the order of the sheath thickness and multiple peaks due to ion–neutral collisions in the sheath are expected to appear. These multiple peaks are apparent in the ion energy distribution for oxygen plasma at 20 mTorr shown in figure 6(c). The mean ion energy increases with decreasing gas pressure, from about 10 eV

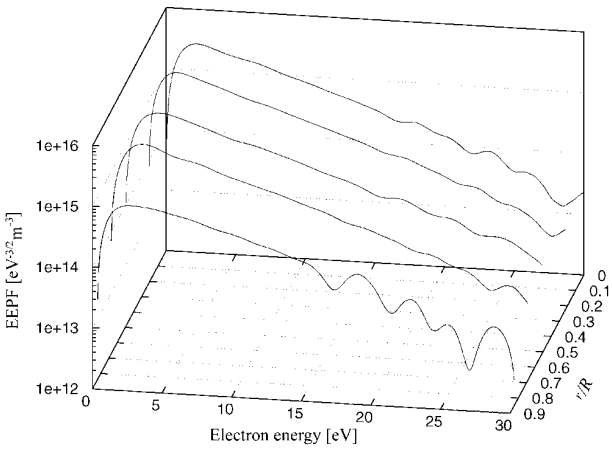

Figure 4. The electron energy probability function in the centre plane of an oxygen discharge at 720 W and 5 mTorr (25 sccm) measured by a Langmuir probe along the radius of the discharge.

at 20 mTorr to roughly 25 eV at 3 mTorr. The mean ion energy follows closely the dc plasma potential measured by a Langmuir probe [11]. Figure 7 shows the variation in the ion intensity with rf power absorbed by the plasma. The O_2^+ ion is the dominant ion in the power and pressure range investigated. This is consistent with other measurements in inductively coupled oxygen discharges [9, 10]. The relative O^+ ion intensity decreases with increased gas pressure.

4. Volume-averaged model

We assume a cylindrical chamber of radius R, length L, volume V and surface area A. A steady flow q of neutral species is introduced through the inlet. The content of the chamber is assumed to be nearly spatially uniform and the power is deposited uniformly into the plasma bulk. We assume an oxygen plasma in which four charged species are present: electrons; O_2^+ created by electron impact ionization of the O_2 molecule and the metastable oxygen molecule $O_2(a\,^1\Delta_g)$; O^+ created by electron impact ionization of oxygen atoms $O(^3P)$ and excited oxygen atoms $O(^1D)$ and O_2 pair creation; and O^- created mainly by dissociative attachment. Negative ions are trapped within the discharge by the positive potential of the plasma with respect to all wall surfaces and are assumed to be lost only by recombination with positive ions and detachment in the volume. The volume-averaged global model is similar to that of Lee *et al* [13] and Lee and Lieberman [14], but has been developed and extended to include more reactions [25] and improvements including self-consistent calculations of the dc plasma potential. The volume reactions included in the global model are listed in table 1.

The plasma chemistry is described by a set of first-order differential equations. For each species a continuity equation describes the creation and the volumetric and surface reactions and losses. For the present study the system of first-order differential equations is allowed to reach a steady state. For neutral species, the main source of O_2 is the flow into the reactor and the neutralization of the O_2^+ ion, while for the creation of O atoms the dissociation of O_2 and recombination of O atoms at the chamber walls play an

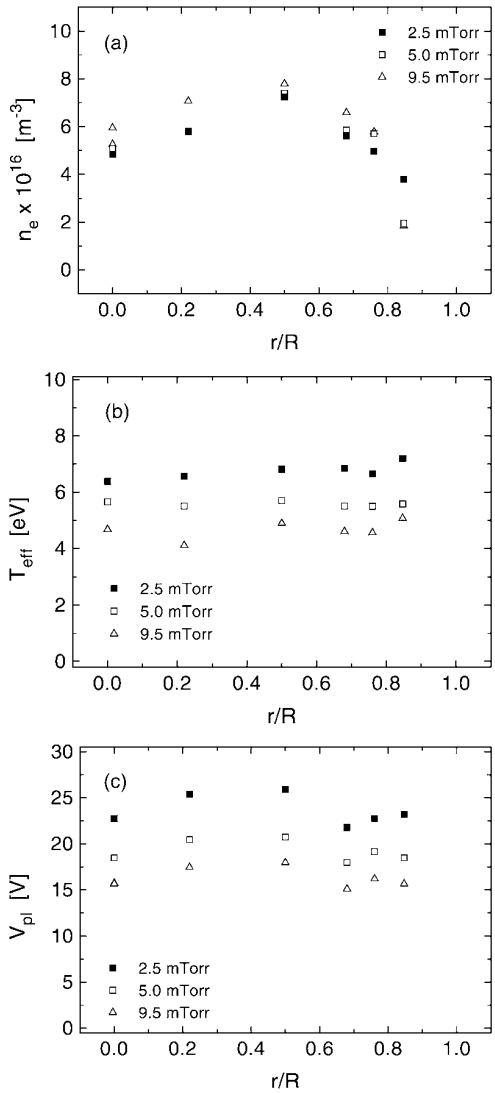

Figure 5. The radial dependence of plasma parameters in an oxygen discharge at 720 W measured by a Langmuir probe: (a) electron density n_e, (b) effective electron temperature T_{eff} and (c) dc plasma potential V_{pl}.

important role. In addition, the charged particle species must satisfy the quasineutrality condition given by

$$n_{O_2^+} + n_{O^+} = n_e + n_{O^-}. \tag{5}$$

The diffusional losses of atomic oxygen $O(^3P)$, the metastable oxygen atoms $O(^1D)$ and metastable oxygen molecules $O_2(a\,^1\Delta_g)$ to the reactor walls are estimated by an effective loss-rate coefficient [28]. The effective loss-rate coefficient for atomic oxygen is given by

$$k_{dl} = \left[\frac{\Lambda_O^2}{D_O} + \frac{2V(2-\gamma_O)}{A v_O \gamma_O}\right]^{-1} \tag{6}$$

where D_O is the neutral diffusion coefficient given by

$$D_O = \frac{eT_g\lambda_i}{v_O m_O} \tag{7}$$

and $v_O = (8eT_g/\pi m_O)^{1/2}$ is the mean neutral speed, γ_O is the sticking coefficient for atomic oxygen on the wall surface;

Table 1. The reaction set for oxygen. The rate constants for electron impact collisions were calculated assuming a Maxwellian electron energy distribution and fit over an electron temperature range of 1–7 eV.

Reaction	Rate coefficient ($m^3\ s^{-1}$)	Reference
$e+O_2 \longrightarrow O_2^+ + 2e$	$k_1 = 9 \times 10^{-16} T_e^2 \exp(-12.6/T_e)$	[13]
$e+O_2^+ \longrightarrow O + O$	$k_2 = 5.2 \times 10^{-15}/T_e$	[5]
$e+O_2 \longrightarrow O(^3P)+O^-$	$k_3 = 8.8 \times 10^{-17} \exp(-4.4/T_e)$	[26]
$e+O(^3P) \longrightarrow O^+ + 2e$	$k_4 = 9.0 \times 10^{-15} T_e^{0.7} \exp(-13.6/T_e)$	[26]
$O^-+O_2^+ \longrightarrow O(^3P)+O_2$	$k_5 = 1.5 \times 10^{-13} (300/T_g)^{1/2}$	[13]
$O^-+O^+ \longrightarrow O(^3P)+O(^3P)$	$k_6 = 2.5 \times 10^{-13} (300/T_g)^{1/2}$	[13]
$e+O^- \longrightarrow O(^3P)+2e$	$k_7 = 2 \times 10^{-13} \exp(-5.5/T_e)$	[26]
$e+O_2 \longrightarrow O(^3P)+O(^3P)+e$	$k_8 = 4.2 \times 10^{-15} \exp(-5.6/T_e)$	[13]
$O+O^- \longrightarrow O_2 + e$	$k_9 = 3.0 \times 10^{-16} (300/T_g)^{1/2}$	[26]
$e+O_2 \longrightarrow O^-+O^+ + e$	$k_{10} = 7.1 \times 10^{-17} T_e^{0.5} \exp(-17/T_e)$	[26]
$e+O_2 \longrightarrow O+O^+ + 2e$	$k_{11} = 5.3 \times 10^{-16} T_e^{0.9} \exp(-20/T_e)$	[26]
$O^+ + O_2 \longrightarrow O(^3P) + O_2^+$	$k_{12} = 2 \times 10^{-17} (300/T_g)^{1/2}$	[4]
$e+O_2 \longrightarrow O(^3P) + O(^1D) + 2e$	$k_{13} = 5 \times 10^{-14} \exp(-8.4/T_e)$	[13]
$e+O(^3P) \longrightarrow O(^1D) + e$	$k_{14} = 4.5 \times 10^{-15} \exp(-2.29/T_e)$	[13]
$O(^1D) + O_2 \longrightarrow O(^3P) + O_2$	$k_{15} = 4.11 \times 10^{-17}$	[13]
$O(^1D) + O \longrightarrow 2O(^3P)$	$k_{16} = 8.1 \times 10^{-18}$	[13]
$e+O(^1D) \longrightarrow O^+ + 2e$	$k_{17} = 9 \times 10^{-15} T_e^{0.7} \exp(-11.6/T_e)$	[13]
$e+O_2 \longrightarrow O_2(a\,^1\Delta_g) + e$	$k_{18} = 1.7 \times 10^{-15} \exp(-3.1/T_e)$	[26]
$e+O_2(a\,^1\Delta_g) \longrightarrow O_2(a\,^1\Delta_g) + 2e$	$k_{19} = 9.0 \times 10^{-16} T_e^2 \exp(-11.6/T_e)$	[26]
$e+O_2(a\,^1\Delta_g) \longrightarrow O^-+O$	$k_{20} = 2.28 \times 10^{-16} \exp(-2.29/T_e)$	[27]
$e+O_2(a\,^1\Delta_g) \longrightarrow O_2 + e$	$k_{21} = 5.6 \times 10^{-15} \exp(-2.2/T_e)$	[26]
$e+O_2(a\,^1\Delta_g) \longrightarrow 2O + e$	$k_{22} = 4.2 \times 10^{-15} \exp(-4.6/T_e)$	[26]
T_g (K)		
T_e (eV)		

V and A are the volume and the wall surface area of the reactor chamber, respectively; and λ_i is the ion-neutral mean free path. The effective diffusion length of each of the neutral species is given by [29]

$$\Lambda_O = \left[\left(\frac{\pi}{L} \right)^2 + \left(\frac{2.405}{R} \right)^2 \right]^{-1/2}. \tag{8}$$

If $\gamma_O \to 1$ the effective loss-rate constant is approximately $k_{dl} \approx D_O/\Lambda_O^2$ and when $\gamma_O \to 0$ then $k_{dl} \approx \frac{1}{4}\gamma_O v_O (A/V)$. The effective loss-rate coefficients for neutrals and positive ions are listed in table 2.

The average electron energy p_e is calculated using the power balance equation, which equates the absorbed power P_{abs} to power losses due to elastic and inelastic collisions and losses due charged particle flow to walls, and is given as

$$\frac{dp_e}{dt} = \frac{P_{abs}}{V} - e\mathcal{E}_c^{(O_2)} k_1 n_{O_2} n_e - k_{23} e(\mathcal{E}_e + \mathcal{E}_i) n_{O_2^+} - e\mathcal{E}_c^{(O)} k_4 n_O n_e - k_{24} e(\mathcal{E}_e + \mathcal{E}_i) n_{O^+} \tag{9}$$

and the electron temperature (in equivalent voltage units) is then

$$T_e = \frac{p_e}{\frac{3}{2} n_e e}. \tag{10}$$

Here $\mathcal{E}_c^{(X)}$ is the energy loss per electron–ion pair created for the neutral X, defined as [12]

$$\mathcal{E}_c = \mathcal{E}_{iz} + \sum_i \mathcal{E}_{ex,i} \frac{k_{ex,i}}{k_{iz}} + \frac{k_{el}}{k_{iz}} \frac{3m_e}{m_i} T_e \tag{11}$$

where $\mathcal{E}_{iz}$ is the ionization energy, $\mathcal{E}_{ex,i}$ is the energy for the ith excitation process, k_{iz} is the ionization rate constant, $k_{ex,i}$ is the rate constant for the ith excited state and k_{el} is the elastic scattering rate constant. The collisional loss $\mathcal{E}_c^{(O_2^+)}$ is the energy lost per electron–O_2^+ ion pair created and is calculated using the excitation rate constants for molecular oxygen given in table 3. The excitation rate constants for molecular oxygen were calculated by integrating the excitation cross sections given by Lawton and Phelps [30] over an assumed Maxwellian electron energy distribution and fit over an electron temperature range of 1–7 eV. The estimated uncertainty of the cross section data is about 25%. Similarly, $\mathcal{E}_c^{(O^+)}$ is the energy loss per electron–O^+ ion pair created. The excitation rate constants for atomic oxygen were calculated by integrating the excitation cross sections given by Laher and Gilmore [31] over an assumed Maxwellian electron energy distribution and fit over an electron temperature range of 1–7 eV. This data has about 50% uncertainty. The rate constants for other excited states of atomic oxygen are given by the rate constant k_h calculated from the total cross sections for excitation of atomic oxygen

Table 2. The interaction coefficients for atomic and molecular oxygen with the reactor walls.

Reaction	Rate coefficient (s^{-1})
$O^+(g) \longrightarrow O(^3P)(g)$	$k_{23} = 2u_{B,O^+}(R^2 h_L + RLh_R)/R^2 L$
$O_2^+(g) \longrightarrow O_2(g)$	$k_{24} = 2u_{B,O_2^+}(R^2 h_L + RLh_R)/R^2 L$
$O(^3P)(g) \longrightarrow \frac{1}{2}O_2(g)$	$k_{25} = \left[\frac{\Lambda_0^2}{D_O} + \frac{2V(2-\gamma_{O^*})}{A v_O \gamma_O} \right]^{-1}$
$O(^1D)(g) \longrightarrow \frac{1}{2}O_2(g)$	$k_{26} = \left[\frac{\Lambda_0^2}{D_{O^*}} + \frac{2V(2-\gamma_{O^*})}{A v_{O^*} \gamma_{O^*}} \right]^{-1}$
$O_2^*(g) \longrightarrow O_2(g)$	$k_{27} = \left[\frac{\Lambda_0^2}{D_{O_2^*}} + \frac{2V(2-\gamma_{O_2^*})}{A v_{O_2^*} \gamma_{O_2^*}} \right]^{-1}$
$O_2^* = O_2(a\,^1\Delta_g)$	

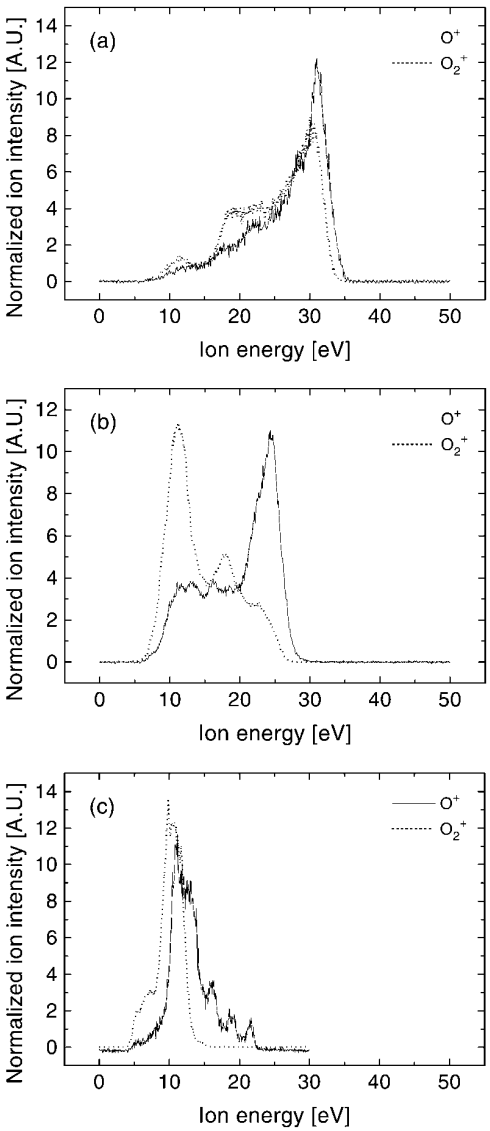

Figure 6. The ion energy distribution in an oxygen discharge at 675 W measured at (a) 3 mTorr (25 sccm), (b) 7 mTorr (25 sccm) and (c) 20 mTorr (85 sccm).

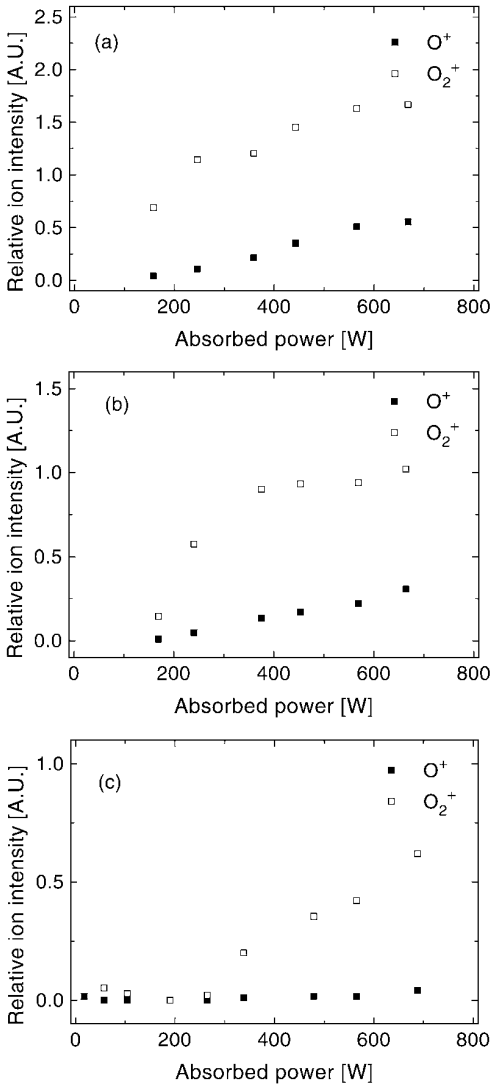

Figure 7. The relative ion intensity for O^+ and O_2^+ ions against absorbed power in an oxygen plasma at (a) 3 mTorr (25 sccm), (b) 7 mTorr (25 sccm) and (c) 20 mTorr (85 sccm).

given by Laher and Gilmore [31] and subtracting the rate constants of all other reactions for atomic oxygen given in the table 3. These highly-excited states are assumed to have threshold energy of approximately 12 eV. The mean ion kinetic energy lost, in equation (10), $\mathcal{E}_i$ is mainly due to the acceleration in the dc potential across the sheath. The ion bombarding energy is thus the sum of the ion energy entering the sheath and the energy gained as it traverses the sheath [32]. The ion velocity entering the sheath is the Bohm velocity $u_B = (eT_e/m_i)^{1/2}$ where m_i is the ion mass, corresponding to a directed energy of $T_e/2$. Hence $\mathcal{E}_i = V_{pl} + \frac{1}{2}T_e$ is the energy acquired by an ion (and hence, lost by the plasma) after falling through the sheath. For electrons that have the Maxwellian electron energy distribution, the mean kinetic energy lost per electron lost is $\mathcal{E}_e = 2T_e$.

The plasma potential V_{pl} at any time is self-consistently calculated by equating the flux loss of positive species (O^+ and O_2^+) to that of the negative species (electrons and O^-) as follows:

$$\Gamma_e + \Gamma_{O^-} = \Gamma_{O^+} + \Gamma_{O_2^+} \tag{12}$$

where

$$\Gamma_{O_2^+} = u_{B_{O_2^+}} \left[\frac{R^2 h_L + RLh_R}{R^2 + RL} \right] n_{O_2^+} \tag{13}$$

$$\Gamma_{O^+} = u_{B_{O^+}} \left[\frac{R^2 h_L + RLh_R}{R^2 + RL} \right] n_{O^+} \tag{14}$$

$$\Gamma_{O^-} = \frac{1}{4} n_{O^-} v_{O^-} \exp\left(-\frac{\phi}{T_{O^-}} \right) \tag{15}$$

$$\Gamma_e = \frac{1}{4} n_e v_e \exp\left(-\frac{\phi}{T_e} \right) \tag{16}$$

where Γ_x is the flux of the corresponding charged species x and ϕ is the potential. Here $u_{B_{O_2^+}}$ and $u_{B_{O^+}}$ are the Bohm velocities for O_2^+ and O^+ ions, respectively. The potential ϕ is equal to the plasma potential V_{pl} when equation (12) is fulfilled. Note that the negative species flux rates are reduced due to the presence of the potential term in the exponent.

Here $v_{O^-} = (8eT_{O^-}/\pi m_O)^{1/2}$ and $v_e = (8eT_e/\pi m_e)^{1/2}$ are the thermal velocities of O^- ions and electrons, respectively. We assume $T_{O^-} = T_i$.

The ratios of the density at the sheath edge to that in the bulk for the axial and radial directions, h_L and h_R respectively, are derived from low-pressure diffusion theory, $(R, L) \geqslant \lambda_i \geqslant (T_i/T_e)(R, L)$, by [33, 34]

$$h_L = \frac{0.86(1+3\alpha/\gamma)}{1+\alpha}\left[3+\frac{L}{2\lambda_i}\right]^{-1/2} \tag{17}$$

$$h_R = \frac{0.8(1+3\alpha/\gamma)}{1+\alpha}\left[4+\frac{R}{\lambda_i}\right]^{-1/2} \tag{18}$$

where λ_i is the ion–neutral mean free path, $\gamma = T_e/T_i$ and $\alpha = n_{O^-}/n_e$. The ion–neutral mean free path is given by

$$\frac{1}{\lambda_i} = \sum_{j=1}^{N_j} n_{g,j}\sigma_{i,j} \tag{19}$$

where $n_{g,j}$ refers to neutral species of the jth ion and $\sigma_{i,j}$ is the ion–neutral scattering cross section for the jth neutral. The neutral gas temperature T_g is assumed to be 600 K. The ion–neutral collision cross section was estimated to be 7.5×10^{-19} m^2 [35].

5. Discussion

The wall recombination coefficient γ_O that appears as a part of k_{25}, k_{26} and k_{27} in table 2 has not been studied extensively for recombination of oxygen. This coefficient determines the ratio of incident oxygen atoms that recombine at the wall. This reaction is the recombination of a gaseous atom with an adsorbed atom on the reactor wall, using the wall surface as a third body:

$$O(g) \longrightarrow \tfrac{1}{2}O_2(g).$$

The recombination coefficient γ_O is a critical parameter in determining the oxygen chemistry or the fractional dissociation as discussed by Lee and Lieberman [14]. For $\gamma_O < 0.01$ they find that pure oxygen plasmas are almost fully dissociated and that O atoms are the dominant neutrals. As γ_O is increased, O_2 molecules play a more important role in the oxygen chemistry, and for $\gamma_O > 0.1$ fractional dissociation is less than 0.5 at 10 mTorr. This factor presumably varies with the wall material, temperature and pressure. In an early study Greaves and Linnett [36] determined that the recombination coefficient γ_O for oxygen atoms on silica to increased from 1.6×10^{-4} at 273 K to 1.4×10^{-2} at 873 K. Booth and Sadeghi [28] estimate the recombination coefficient to be roughly 0.5 for oxygen atoms on stainless-steel. For this work the recombination coefficient is assumed to be $\gamma_O = 1$ for oxygen. It was noticed that the pressure in the chamber after plasma ignition did not change much, indicating that there was little dissociation or that the wall recombination of O atoms is high. This is supported by the fact that the ion stream arriving to the mass spectrometer consisted predominantly of O_2^+ ions. Since ionization of atomic oxygen is the main source of atomic oxygen ions, this suggests a high wall recombination.

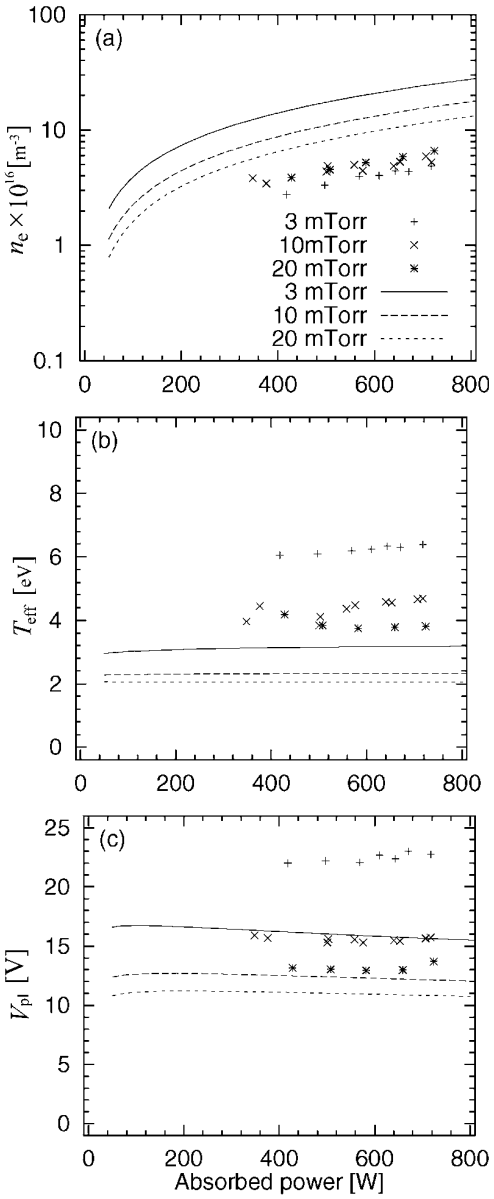

Figure 8. (a) The electron density, (b) the effective electron temperature and (c) the dc plasma potential against absorbed power in an oxygen plasma at various gas pressures, measured with a Langmuir probe at: +, 3 mTorr (10 sccm); ×, 10 mTorr (25 sccm) and ∗, 20 mTorr (50 sccm); compared to global model (volume-averaged) calculations.

The results of the Langmuir probe and QMS ion measurements are compared with the model in figures 8 and 9. Figure 8(a) compares model densities with Langmuir probe measurements at 3, 10 and 20 mTorr over the power range 100–800 W. The measured electron density is in the range 3×10^{16}–7×10^{16} m^{-3} and increases with increasing power and pressure. The measured electron density is a factor of three to six lower than the model prediction, but follows the same trend; increases linearly with increased power. The fraction of O^+ ions in the oxygen discharge, defined as $[O^+]/([O_2^+]+[O^+])$, obtained from the mass spectrometer is compared to the model in figure 9. The $[O^+]/([O_2^+]+[O^+])$ ratio increases with increased power and decreases with increased gas pressure. Tuszewski *et al* [9, 10] found a

Table 3. Rate constants for excitation of atomic and molecular oxygen. The rate constants were calculated by integrating the excitation cross sections over an assumed Maxwellian electron energy distribution function and fit over an electron temperature range of 1–7 eV.

Reaction	Threshold (eV)	Rate coefficient ($m^3\ s^{-1}$)
Atomic oxygen		
$e+O(^3P) \longrightarrow O(^1D) + e$	1.96	$k_{1_D} = 4.47 \times 10^{-15} \exp(-2.286/T_e)$
$e+O(^3P) \longrightarrow O(^1S) + e$	4.18	$k_{1_S} = 4.54 \times 10^{-15} \exp(-4.49/T_e)$
$e+O(^3P) \longrightarrow O(^5S^o) + e$	9.14	$k_{5_S} = 9.67 \times 10^{-16} \exp(-9.97/T_e)$
$e+O(^3P) \longrightarrow O(^3S^o) + e$	9.51	$k_{3_S} = 9.67 \times 10^{-16} \exp(-9.75/T_e)$
$e+O(^3P) \longrightarrow O^h + e$	12.0	$k_h = 4.31 \times 10^{-14} \exp(-18.6/T_e)$
$e+O(^3P) \longrightarrow O(^3P^o) + e$	15.65	$k_{3_{Po}} = 4.54 \times 10^{-15} \exp(-17.34/T_e)$
Molecular oxygen		
$e+O_2(r=0) \longrightarrow O_2(r>0) + e$	0.02	$k_{rot} = 0$
$e+O_2(v=0) \longrightarrow O_2(v=1) + e$	0.19	$k_{v=1} = 2.8 \times 10^{-15} \exp(-3.72/T_e)$
$e+O_2(v=0) \longrightarrow O_2(v=2) + e$	0.38	$k_{v=2} = 1.28 \times 10^{-15} \exp(-3.67/T_e)$
$e+O_2(X\,^3\Sigma_g^-) \longrightarrow O_2(a\,^1\Delta_g) + e$	0.977	$k_{a\,^1\Delta_g} = 1.37 \times 10^{-15} \exp(-2.14/T_e)$
$e+O_2(X\,^3\Sigma_g^-) \longrightarrow O_2(b^1\Sigma_g^+) + e$	1.627	$k_{b\,^1\Sigma_g^+} = 3.24 \times 10^{-16} \exp(-2.218/T_e)$
$e+O_2(X\,^3\Sigma_g^-) \longrightarrow O_2(ex1) + e$	4.5	$k_{ex1} = 1.07 \times 10^{-15} \exp(-3.43/T_e)$
$e+O_2(X\,^3\Sigma_g^-) \longrightarrow O_2(1dis) + e$	6.0	$k_{1dis} = 3.73 \times 10^{-15} \exp(-4.9/T_e)$
$e+O_2(X\,^3\Sigma_g^-) \longrightarrow O_2(2dis) + e$	8.4	$k_{2dis} = 3.91 \times 10^{-14} \exp(-8.29/T_e)$
$e+O_2(X\,^3\Sigma_g^-) \longrightarrow O_2(3dis) + e$	9.97	$k_{3dis} = 1.92 \times 10^{-16} \exp(-11.48/T_e)$
$e+O_2(X\,^3\Sigma_g^-) \longrightarrow O_2(ex2) + e$	14.7	$k_{ex2} = 1.13 \times 10^{-15} \exp(-18.35/T_e)$

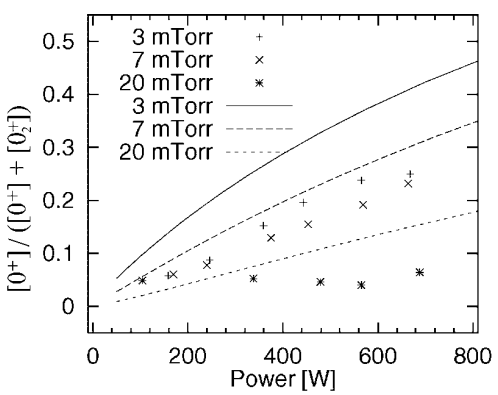

Figure 9. Fraction of O^+ ions in an oxygen discharge as a function of the power for various gas pressures. The measured values (dots) are compared to global (volume-averaged) model calculations (curves).

similar dependence of $[O^+]/([O_2^+]+[O^+])$ on pressure and power. If we assume creation of O atoms is mainly due to dissociation and neutralization and the loss is due to recombination at the wall and pumping out of the system we can write $(k_3 + 2k_8)n_{O_2}n_e \approx k_{16}n_O + (S/V)n_O$ or $n_O/n_{O_2} \propto n_e \propto P_{abs}$ which indicates that dissociation increases with increased power. The ion ratio $n_O^+/n_{O_2^+}$ scales in similar way since the ion concentration is roughly a balance between ionization and loss of charged particles to the chamber walls. It should be noted that multiple peaks in the measured ion energy distribution at 20 mTorr (see figure 6(c)) for both O^+ and O_2^+ ions indicate collisions in the sheath. Thus the $[O^+]/([O_2^+]+[O^+])$ ratio measured (and shown in figure 9) may not represent the bulk properties at 20 mTorr.

The electron temperature predicted by the model calculations is compared to the effective electron temperature T_{eff} measured by the Langmuir probe figure 8(b). The measured value is consistently larger than the value predicted by the model. The dc plasma potential as measured by the Langmuir probe and predicted by the global model is shown in figure 8(c). The measured plasma potential decreases with increasing pressure, is about 22 V at 3 mTorr and falls to about 13 V at 20 mTorr. This is consistent with other reported values of the plasma potential in inductive discharges [6, 9]. Comparison of the effective electron temperature T_{eff} in a planar inductive oxygen discharge measured by different groups is shown in table 4. Since the effective electron temperature is essentially a function of the discharge gas pressure, it should be comparable [8]. The electron density, however, depends on the power applied and the discharge geometry. We note that the measured effective electron temperature reported in this work is comparable to the values reported by Barnes *et al* [6].

Table 4. Comparison of effective electron temperature in a planar inductive oxygen discharge measured by different groups.

			T_{eff} (eV)	
Reference	R (cm)	L (cm)	5 mTorr	10 mTorr
Barnes *et al* [6]	10.2	7.6	5.1	4.5
Schwabedissen *et al* [8]	12.4	4.1	9.3	6.8
This work	15.2	7.6	5.4	4.4

The electron energy probability function for oxygen plasma at roughly 720 W absorbed power is shown in figure 2. The electron energy distribution shows Maxwellian behaviour for low electron energy. At higher electron energy the electron energy distribution function is depleted due to inelastic interaction as well as escape of high-energy electrons from the bulk to the chamber walls. Similar depletion at high electron energy is reported by Schwabedissen *et al* [8] and Barnes *et al* [6] in a planar oxygen discharge. In the global model the electron energy distribution function is assumed to be Maxwellian. The distributions shown in figure 2 for our inductive discharge show that this is a good assumption. However, Schwabedissen *et al* [8] indeed point out that the underpopulation of the EEDF at high electron energy may

cause significant error in the calculation of excitation and ionization rates in non-Maxwellian plasmas.

6. Conclusions

A Langmuir probe and a QMS were used to determine the plasma parameters of an oxygen plasma in a planar inductive discharge. The electron density, effective electron temperature, dc plasma potential and the electron energy probability function in the discharge centre plane were investigated as a function of power, gas pressure and radial position. A volume-averaged global model of electronegative oxygen discharge was developed. The model uses a power balance equation to account for energy deposited into the plasma and lost via collisions and particle flux. The particle densities are modelled via rate equations estimated from collision cross sections assuming Maxwellian electron energy distribution functions. The volume-averaged model is shown to predict the experimental trends over a range of process conditions. However, the effective electron temperature is underestimated by a factor of two by the global model and the electron density overestimated by a factor of three to six. This may be due to the depletion at high electron energy compared to the Maxwellian electron energy distribution assumed in the model. Furthermore, the positive ion flux to the discharge walls depends on the sheath edge density. Equations (17) and (18), for the sheath edge to centre ion density, are modified versions of equations derived by Godyak and Maximov [33] and Godyak [34] for electropositive plane parallel discharge and infinitely long cylindrical discharge, respectively. Oxygen discharges are electronegative and therefore the equations must be generalized to include the transitions from electropositive to electronegative regions [37]. Appropriate theory remains to be developed and the influence of this approximation to be investigated. It should be noted that there is a significant uncertainty, up to 50%, on the measured excitation cross sections data and many of the cross sections for binary processes among the species have not been carefully measured or calculated. These issues along with the validity of limited reaction sets will be the subject of future study.

Acknowledgments

This work was partially supported by the Icelandic Research Council, NSF Grant ECS-9820836, the Lam Research Corporation, California Industries and the State of California UC-SMART Program under contract 97-01.

References

[1] Tolliver D L 1984 *VLSI Electronics: Microstructure Science* vol 8, ed N G Einspruch and D M Brown (Orlando, FL: Academic) pp 1–24
[2] Carl D A, Hess D W, Lieberman M A, Nguyen T D and Gronsky R 1991 *J. Appl. Phys.* **70** 3301
[3] Kitajima M, Kuroki H, Shinno H and Nakamura K G 1992 *Solid State Commun.* **83** 385
[4] Elíasson B and Kogelshatz U 1986 Basic data for modelling of electrical discharges in gases: oxygen *Report* KLR-11C, Brown Boveri Konzernforschung, CH5405, Baden
[5] Kossyi I A, Kostinsky A Y, Matveyev A A and Silakov V P 1992 *Plasma Sources Sci. Technol.* **1** 207
[6] Barnes M S, Forster J C and Keller J H 1993 *Appl. Phys. Lett.* **62** 2622
[7] Keller J, Forster J and Barnes M 1993 *J. Vac. Sci. Technol.* A **11** 2487
[8] Schwabedissen A, Benck E C and Roberts J R 1997 *Phys. Rev.* E **55** 3450
[9] Tuszewski M, Scheuer T J and Tobin J A 1995 *J. Vac. Sci. Technol.* A **13** 839
[10] Tuszewski M 1996 *J. Appl. Phys.* **79** 8967
[11] Gudmundsson J T 1999 *J. Phys. D: Appl. Phys.* **32** 798
[12] Lieberman M A and Gottscho R A 1994 *Physics of Thin Films* vol 18, ed M Francombe and J Vossen (New York: Academic) pp 1–119
[13] Lee C, Graves D B, Lieberman M A and Hess D W 1994 *J. Electrochem. Soc.* **141** 1546
[14] Lee C and Lieberman M A 1995 *J. Vac. Sci. Technol.* A **13** 368
[15] Wainman P N, Lieberman M A, Lichtenberg A, Stewart R and Lee C 1995 *J. Vac. Sci. Technol.* A **13** 2464
[16] Gudmundsson J T, Kimura T and Lieberman M A 1999 *Plasma Sources Sci. Technol.* **8** 22
[17] Godyak V A, Piejak R B and Alexandrovich B M 1992 *Plasma Sources Sci. Technol.* **1** 36
[18] Gudmundsson J T 1997 On smoothing of the *I–V* Langmuir probe characteristic *Memorandum* No UCB/ERL M97/38, Electron Research Laboratory, University of California, Berkeley, USA
[19] Druyvesteyn M J 1930 *Z. Phys.* **64** 781
[20] Lieberman M A and Lichtenberg A J 1994 *Principles of Plasma Discharges and Materials Processing* (New York: Wiley) p 177
[21] Grant R B 1987 *J. Vac. Sci. Technol.* **5** 2428
[22] Hopwood J, Guarnieri C R, Whitehair S J and Cuomo J J 1993 *J. Vac. Sci. Technol.* A **11** 147
[23] Meyer J A and Wendt A E 1995 *J. Appl. Phys.* **78** 90
[24] Meyer J A, Mau R and Wendt A E 1996 *J. Appl. Phys.* **79** 1298
[25] Patel K K 1998 *Master's Thesis* University of California at Berkeley
[26] Lieberman M A and Lichtenberg A J 1994 *Principles of Plasma Discharges and Materials Processing* (New York: Wiley) pp 251–6
[27] Burrow P D 1973 *J. Chem. Phys.* **59** 4922
[28] Booth J P and Sadeghi N 1991 *J. Appl. Phys.* **70** 611
[29] Chantry P J 1987 *J. Appl. Phys.* **62** 1141
[30] Lawton S A and Phelps A V 1978 *J. Chem. Phys.* **69** 1055
[31] Laher R R and Gilmore F R 1990 *J. Phys. Chem. Ref. Data* **19** 277
[32] Lieberman M A and Lichtenberg A J 1994 *Principles of Plasma Discharges and Materials Processing* (New York: Wiley) pp 304–7
[33] Godyak V A and Maximov V N 1977 *Vestnik Moskovskogo Universiteta, ser. Physica i Astronomia* **18** 51
[34] Godyak V 1986 *Soviet Radio Frequency Discharge Research* (Falls Church, VA: Delphic Associates)
[35] Hickman A P, Medikeri-Naphade M, Chapin C D and Huestis D L 1997 *Geophys. Res. Lett.* **24** 119
[36] Greaves J C and Linnett J W 1959 *Trans. Faraday Soc.* **55** 1355
[37] Kouznetsov I G, Lichtenberg A J and Lieberman M A 1996 *Plasma Sources Sci. Technol.* **5** 662